Quantum-Dot-Based Förster Resonance Energy Transfer Immunoassay for Sensitive Clinical Diagnostics of Low-Volume Serum Samples

K. David Wegner,[†] Zongwen Jin,[†] Stina Lindén,[†] Travis L. Jennings,[‡] and Niko Hildebrandt[†,*]

[†]Institut d'Electronique Fondamentale, Université Paris-Sud, 91405 Orsay Cedex, France and [‡]eBioscience, Inc., 10255 Science Center Drive, San Diego, California 92121, United States

ABSTRACT A myriad of quantum dot (QD) biosensor examples have emerged from the literature over the past decade, but despite their photophysical advantages, QDs have yet to find acceptance as standard fluorescent reagents in clinical diagnostics. Lack of reproducible, stable, and robust immunoassays using easily prepared QD-antibody conjugates has historically plagued this field, preventing researchers from advancing the deeper issues concerning assay sensitivity and clinically relevant detection limits on low-volume serum samples. Here we demonstrate a ratiometric multiplexable FRET immunoassay using Tb donors and QD acceptors, which overcomes all the aforementioned limitations toward application in clinical diagnostics. We demonstrate the determination of prostate specific antigen (PSA) in 50 μL serum samples with subnanomolar (1.6 ng/mL) detection limits using time-gated detection and two different QD colors. This concentration is well below the clinical cutoff value of PSA, which demonstrates the possibility of direct integration into real-life *in vitro* diagnostics. The application of IgG, F(ab')$_2$, and F(ab) antibodies makes our homogeneous immunoassay highly flexible and ready-to-use for the sensitive and specific homogeneous detection of many different biomarkers.

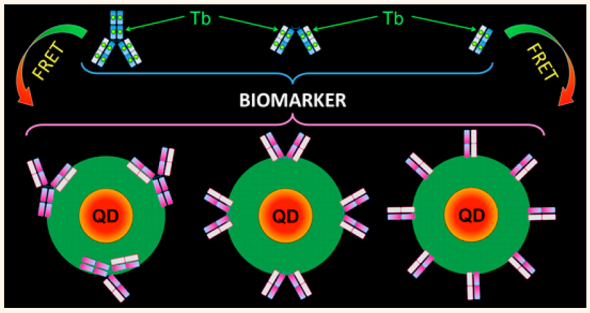

KEYWORDS: FRET · quantum dot · terbium · multiplexing · immunoassay · PSA · diagnostics

Next generation molecular diagnostics platforms are focusing on emerging technologies capable of providing rapid assays with enhanced sensitivity and efficient multiplexing performance for biomarker detection.[1] A major driving force is the desire to realize the goals of personalized medicine and point-of-care testing under clinically relevant conditions, especially for biomarkers found in blood, serum, or plasma.[2] Nanobiophotonics, which couples the speed and sensitivity of luminescence with the ultrasmall dimensions of nanoparticles,[3] and in particular colloidal quantum dots (QDs), is in a competitive position to meet the challenging requirements of multiplexed *in vitro* diagnostics (IVD). Although QDs offer distinct advantages in photostability with high brightness and color tunability if used in appropriate solvents,[4−14] they have yet to gain acceptance into standard clinical practice as reporter tags, due largely to either physical or chemical stability issues or insufficient sensitivity in biological media such as serum or plasma.[15] A highly specific QD bioconjugate capable of preserving its advantageous optical properties within such indispensable clinical sample matrices would be of immense utility toward meeting IVD criteria.

Tb-to-QD Förster resonance energy transfer (FRET) has proven itself to be an efficient tool for spectro-temporal multiplexing, offering several unique advantages over organic dye-based FRET systems for biomolecular sensing.[16−21] For specific and sensitive biomarker detection in homogeneous sandwich assays, antibodies remain the biomolecule of choice. However, the combination of QDs with antibodies has yet to be established within this context. Such developments have been hindered by insufficient labeling chemistries and the large donor−acceptor distances, which result from

* Address correspondence to niko.hildebrandt@u-psud.fr.

Received for review June 26, 2013 and accepted August 2, 2013.

Published online August 02, 2013
10.1021/nn403253y

the thick surface coatings of commercial QDs. Still, these commercial polymer/lipid-based coatings are indispensable for maintaining bright and stable QDs in clinical media such as serum or plasma. Although it has been shown that QDs can be used in FRET-based immunoassays,[22−31] these assays were heterogeneous, competitive, and/or nonratiometric, and, most importantly, measured in buffer systems instead of in serum. Serum validation is essential if QD-based immunoassays are to be accepted for IVD use, and so we found it helpful to list the traits for what may be considered the "ideal" immunoassay:

(1) *homogeneous* (no washing and separation steps)
(2) *serum-based* (human serum samples)
(3) *sensitive* (clinically relevant detection limits)
(4) *specific* (use of at least two primary antibodies for target binding)
(5) *fast* (liquid phase binding kinetics and quick measurement)
(6) *small* (small sample volumes below 100 μL)
(7) *reproducible* (ratiometric measurement in order to correct for medium interferences)
(8) *robust* (stable performance independent of individual user or environment)
(9) *flexible* (universal format for many biomarkers, facile conjugate production/purification)
(10) *multiplexed* (simultaneous measurement of several biomarkers)
(11) *stable* (long-term stability and shelf life).

In the QD-based biosensor presented here, we demonstrate that, by thoughtful design changes, we were able to develop such an ideal immunoassay attaining clinically relevant limits of detection (1.6 ng/mL) on prostate specific antigen (PSA) in 50 μL serum samples using commercial reagents and instrumentation.

RESULTS AND DISCUSSION

Flexible Antibody Conjugation and Purification. To date, FRET sandwich immunoassays using commercially available, stable, and biocompatible polymer/lipid embedded QDs (*e.g.*, Life Technologies or eBioscience) have not been realized. This is due to the limited distance range for QD−dye FRET pairs and the large donor−acceptor distance within such a sandwich complex. The complex in this scenario is composed of a QD with a thick surface coating (*ca.* 15 nm diameter), a first antibody (AB, *ca.* 150 kDa corresponding to a length of approximately 10 nm for the Y-shaped IgG), a biomarker (different sizes, *e.g.*, 34 kDa or *ca.* 2 nm for PSA), and finally a second AB with the reporter tag. The total distance between the QD and reporter fluorophore may be between ~15 and 30 nm, which is well beyond the measurable distance range of 5−10 nm for traditional FRET pairs. We solve the dilemma of these physical limitations with a two-pronged approach: (1) increasing the effective measurable energy transfer range to ~20 nm by time-gated Tb-to-QD FRET and (2) decreasing AB sizes from full IgG (*ca.* 150 kDa) to reduced F(ab′)$_2$ (*ca.* 100 kDa) and further to F(ab) (*ca.* 50 kDa) fragments of two different monoclonal primary antibodies against PSA to bring the Tb closer to the central QD. These two design modifications combine to make a system that is more compact in separation distance and more efficient in energy transfer, thereby enabling the potential for a homogeneous QD-based FRET immunoassay. The fulfillment of this compact design relies heavily upon the successful formation of different AB fragments and optimizing conjugation chemistry for bioconjugate assembly.

TABLE 1. Tb Donor/QD Acceptor Ratios for the Different Sandwich Immunoassays[a]

Tb-AB\QD-AB	QD-IgG	QD-F(ab′)$_2$	QD-F(ab)
Tb-IgG	31	56	210
Tb-F(ab′)$_2$	23	40	150
Tb-F(ab)	9.4	17	62

[a] Calculated ratios of Tb/QD in a theoretical sandwich immunoassay based on the measured Tb/AB and AB/QD ratios after conjugation to the different formats. Calculations are based on a linear model of combination, disregarding divalency of IgG or F(ab′)$_2$ and the effects of steric hindrance. The calculated values are meant purely as a guide for the eye to show the complex with the highest potential ratio of Tb/QD, which would in turn be the most sensitive (lowest detection limit) immunoassay.

The relatively small Tb complexes (NHS-activated Lumi4-Tb [Tb] delivered in lyophilized form for long-term storage, Lumiphore, Inc.)[32] were conjugated in a straightforward manner *via* coupling of NHS-activated Tb to available primary amines of the ABs.[33] AB coupling to the QD nanocrystals was accomplished using sulfhydryl-reactive conjugation chemistry as described in detail elsewhere[34] (eFluor 650NC [QD650] conjugation kits, eBioscience, Inc.). Labeling ratios of the Tb and QD conjugates were determined by UV/vis absorption spectroscopy as 13 Tb/IgG, 9.4 Tb/F(ab′)$_2$, 3.9 Tb/F(ab), 2.4 IgG/QD650, 4.3 F(ab′)$_2$/QD650, and 16 F(ab)/QD650 (with a determination error of ±30%). This shows that the Tb/AB labeling ratio decreases and AB/QD labeling increases with decreasing AB size, as expected from the size comparison of the different components (cf. Scheme 1). Based on these measured ratios, Table 1 calculates the theoretical number of Tb per QD for the different combinations. Clearly, the scenario combining the QD-F(ab) conjugate with the Tb-IgG sensitizer would be expected to yield the highest Tb/QD ratio and thus the highest proportion of Tb-to-QD FRET because the large difference in excited-state lifetimes (2.3 ms for Tb and few tens of nanoseconds for QD) allows the excitation of one QD by multiple Tb in a serial manner assuming there is enough excitation energy for multiple Tb (which is reasonable for the pulsed laser excitation).[35] This higher overall brightness of the FRET system (more QD emission intensity per QD due to FRET sensitization by multiple Tb) is also expected to lead to a higher sensitivity of the immunoassay.[20] Apart from a

possible higher FRET efficiency, the smaller ABs for QD conjugation have another important advantage, namely, an easier (QD-AB) conjugate purification (which is much more problematic for QD/IgG conjugates which are similar in size) by convenient spin column separation. One problem of high labeling ratios might be steric hindrance. The conjugation of *ca.* 16 F(ab) fragments in a random orientation on the QD surface might lead to inaccessibility of some F(ab)s to Tb-ABs *via* PSA binding, especially when the ABs are the relatively large IgGs. As would be expected from the Tb/QD ratio (Table 1), larger ABs for QDs combined with smaller ABs for Tb were disadvantageous (*e.g.*, QD-IgG and Tb-F(ab) lead to few large ABs on the QD and a low labeling ratio of Tb on small ABs; this results in the disadvantageous situation of large donor–acceptor distances and only few donor–acceptor pairs) and are therefore not treated further within this study.

In order to demonstrate the multiplexability of our FRET assay by using different QD colors, we also labeled IgG antibodies to QD605 (eFluor 605NC, eBioscience) with an approximate labeling ratio of 0.5 ± 0.3 IgG/QD605. The lower the labeling ratio, the higher the probability to have a significant amount of unconjugated QDs (assuming a Poisson distribution of labeling), which cannot participate in FRET. However, due to the very long excited-state lifetimes of Tb, incomplete labeling is not problematic for FRET-based assays.[21] Unconjugated QDs provide a short-lived luminescence signal, which is not specific for binding to a biomarker and which contributes only very few background signals that are largely suppressed due to time-gated detection in the millisecond range. FRET-sensitized QD emission can only be caused by binding with Tb-ABs *via* PSA and is therefore specific for PSA. This luminescence is long-lived (due to sensitization by long-lived Tb) and can therefore be efficiently distinguished from the short-lived luminescence of unlabeled QDs.

Optical Characterization of the FRET Assays. The photophysical properties (Figure 1) of Tb and QD were not influenced by AB conjugation. The broad overlap of the Tb emission and the QD absorption (Figure 1) combined with the large QD molar absorptivity values (especially for QD650) leads to very long Förster distances (donor–acceptor distance of 50% FRET efficiency), calculated as $R_0 = 0.02108\ (\kappa^2 \Phi_{Tb} n^{-4} J)^{1/6}$ nm, with the FRET orientation factor $\kappa^2 = 2/3$, the Tb-centered luminescence quantum yield $\Phi_{Tb} = 0.67 \pm 0.5$, the refractive index $n = 1.35$, and the overlap integral $J = \int F_{Tb} \varepsilon_{QD} \lambda^4 d\lambda$ (from 450 to 700 nm with the area-normalized Tb emission spectrum F_{Tb} and the QD molar absorptivity spectra ε_{QD}; cf. Figure 1). These values were $R_0 = 10.7 \pm 0.5$ nm and $R_0 = 7.7 \pm 0.3$ nm for the Tb-QD650 and Tb-QD605 FRET pairs, respectively. Taking into account that FRET is measurable between *ca.* 0.5 and 2 times R_0, these large Förster distances increase the FRET range to distances of

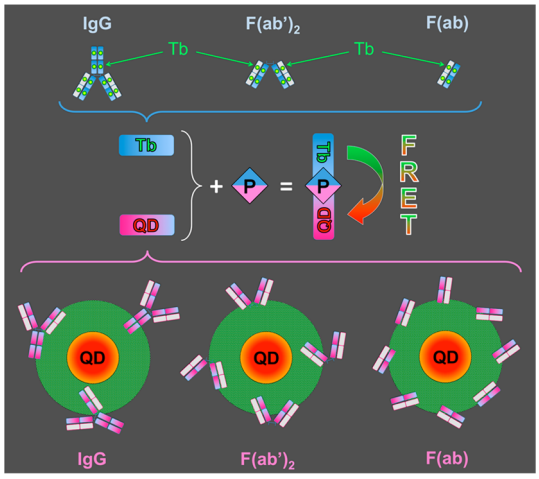

Scheme 1. Principle of the QD-based homogeneous FRET immunoassay. Tb-antibody conjugates (top) and QD-antibody conjugates (bottom) contain each a different primary antibody (which are further reduced to F(ab′)$_2$ and F(ab) fragments) against PSA. All possible combinations of the six different conjugates were used to specifically recognize PSA (P) in FRET sandwich immunoassays (center).

up to approximately 20 nm. Such Tb-to-QD FRET systems follow quite well the classical r^{-6} distance-dependent FRET model and have been studied extensively before.[17,18,20,21,35–40]

All FRET assays contained 50 μL of each AB conjugate (Tb and QD) at constant concentrations to which 50 μL of serum with increasing concentrations of PSA was added. For the QD650, all possible AB configurations from Scheme 1 were used. For QD605 (which served to demonstrate the capability of multiplexing), only the IgG conjugates were applied. The Tb donor to QD acceptor distance (r_{DA}) is expected to be quite large due to two different antibodies, the PSA antigen and the thick QD coating. As mentioned above, the system using two IgGs could easily lead to r_{DA} values of ~15 to 30 nm. In fact, an exact r_{DA} estimation is extremely difficult because many distance-determining factors need to be taken into account: (1) the application of IgGs and smaller F(ab′)$_2$ and F(ab) fragments, (2) a random orientation and distribution of the acceptor ABs on the QDs (as depicted in Scheme 1), (3) a random distribution of several Tb over the donor ABs, and (4) the various possible orientations and distances of the Tb-ABs to the QD due to the flexibility of the "(Tb-AB)-PSA-(QD-AB)" binding and sterical hindrance problems for highly labeled systems. Assuming a diameter of 14 nm for the QD650,[40] and a Tb-AB on the surface of the QD (due to the binding flexibility mentioned above), the minimum r_{DA} value would be approximately 7 nm. The maximum distance would be caused by an elongated "(Tb-IgG)-PSA(QD-IgG)" system with Tb and QD on opposite ends. This scenario would lead to a maximum r_{DA} value of *ca.* 29 nm (10 nm IgG + 2 nm PSA + 10 nm IgG + 7 nm QD radius). Using the

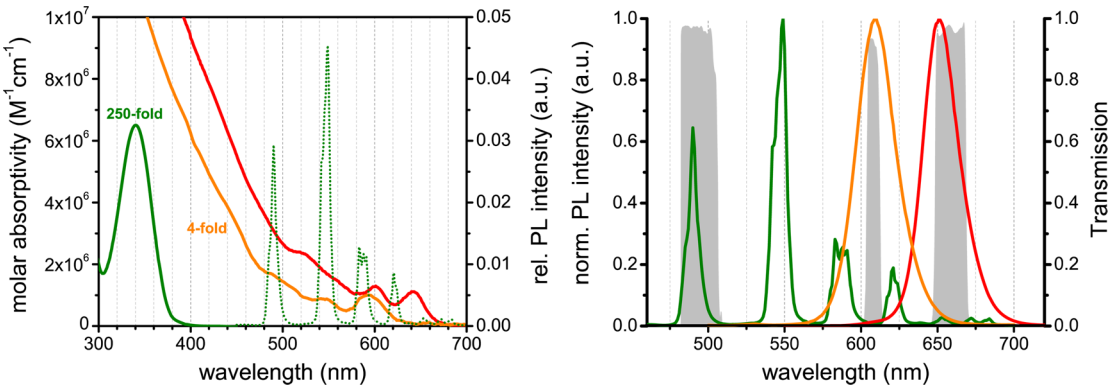

Figure 1. Optical properties of the FRET assay components. Left: Molar absorptivity spectra of Tb (green, multiplied by 250), QD605 (orange, multiplied by 4), and QD650 (red). For the calculation of the overlap integrals between Tb donor emission and QD acceptor absorption, the area-normalized Tb emission spectrum (green dotted) is also shown. Right: Photoluminescence (PL) intensity spectra of Tb (green), QD605 (orange), and QD650 (red) antibody conjugates normalized to unity at their respective maxima. The gray spectra in the background define the transmission of the optical band-pass filters within the Tb (494 ± 20 nm), QD605 (607 ± 8 nm), and QD650 (660 ± 13 nm) detection channels. Tb-centered, QD605, and QD650 PL quantum yields are 0.67 ± 0.5, 0.70 ± 0.07, and 0.55 ± 0.07, respectively.

Förster distance of $R_0 = 10.7$ nm and the FRET efficiency (η_{FRET}) calculated by

$$\eta_{FRET} = \frac{{R_0}^6}{{R_0}^6 + {r_{DA}}^6} = 1 - \frac{\tau_{DA}}{\tau_D} \qquad (1)$$

with the photoluminescence (PL) decay times of pure Tb-AB (τ_D = 2.3 ms) and of the FRET pair (τ_{DA}) leads to FRET efficiencies of η_{FRET}(max) = 0.92 and η_{FRET}(min) = 0.0025 and FRET decay times of τ_{DA}(min) = 0.17 ms and τ_{DA}(max) = 2.3 ms. As all donor−acceptor distances between 7 and 29 nm are possible, one would expect PL decay curves with a decay time distribution ranging from *ca.* 0.17 ms (maximum FRET) to *ca.* 2.3 ms (minimum FRET or emission from unquenched Tb).

Pulsed excitation with 337 nm (in the absorption maximum of Tb; cf. Figure 1) leads to excited-state Tb and QD and PL decay curves as those shown in Figure 2 for the F(ab′)$_2$ conjugates of Tb and QD650 (the PL decay curves for the other systems are shown in the Supporting Information). The PL decay curves of PSA-containing assays (6, 12, and 24 nM shown as representative curves) acquired in the QD detection channel show higher PL intensities (sensitization) and new decay time components, originating from FRET sensitization, compared to the PL decay curve of the assay containing no PSA (black curve). In agreement with the QD sensitization, the Tb detection channel shows a concomitant FRET quenching in intensity and decay time. Although the single PL decay time components cannot be determined from these decay curves, both the QD-sensitized and the Tb-quenched decay curves reveal new decay components in the expected range from *ca.* 0.17 to 2.3 ms. Thus, the PL decay curves give clear evidence of FRET from Tb (FRET-quenched) to QD (FRET-sensitized) upon PSA recognition by the antibody conjugates (formation of "(Tb-AB)-PSA-(QD-AB)" sandwich complexes).

Another interesting aspect can be found in the comparison of the PL decay curves of the different FRET systems in the Tb detection channel. Within the QD-F(ab′)$_2$-containing systems (Figure 2 and Figure S2), the FRET quenching (new shorter decay components) becomes much more obvious than for the systems containing QD-IgG or QD-F(ab) (Figures S1, S3, S4, and S5), for which only a slight intensity increase can be detected. For the IgG systems, we attribute this behavior to many Tb-QD pairs at very long distances leading to a large majority of unquenched Tb. In the case of the F(ab) systems, the large labeling ratio and the small F(ab) fragments on the QD might lead to steric hindrance, preventing the formation of "(Tb-IgG)-PSA-(QD-F(ab))" sandwich complexes and leading to a large amount of unbound Tb-IgG, which leads to an excess of unquenched Tb. Reduced affinity of the F(ab) fragments compared to the full IgGs could be another reason for the reduced PL quenching.

Homogeneous FRET Immunoassays for PSA. The homogeneous FRET immunoassays were measured on a KRYPTOR compact plus (Cezanne/Thermo Fisher Scientific) clinical fluorescence plate reader, which simultaneously detects the time-gated PL intensities (integration of the PL intensities within the time window from 0.1 to 0.9 ms after pulsed excitation) in the Tb donor and the QD acceptor channels (cf. filter transmission spectra in Figure 1 for wavelength ranges of these two channels). This time-gating allows very efficient suppression of the short-lived sample autofluorescence and of the very strong fluorescence from directly excited QDs. The time-gated intensities in the QD acceptor channel I_{QD}(0.1−0.9 ms) and the Tb donor channel I_{Tb}(0.1−0.9 ms) are used to calculate the FRET ratio F_R (FRET sensitization divided by FRET quenching):

$$F_R = \frac{I_{QD}(0.1 - 0.9\ \text{ms})}{I_{Tb}(0.1 - 0.9\ \text{ms})} \qquad (2)$$

F_R is used for the determination of the biomarker concentration and leads to very low coefficients of variation

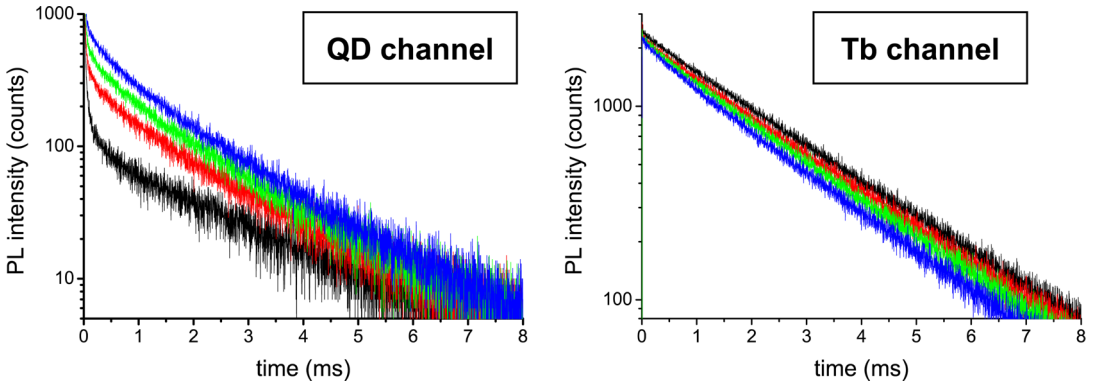

Figure 2. PL decay curves of the "(Tb-F(ab′)$_2$)-PSA-(QD650-F(ab′)$_2$)" FRET immunoassays. The addition of 50 μL serum containing increasing PSA concentrations (black, no PSA; red, 6 nM; green, 12 nM; blue, 24 nM) to a 100 μL solution of Tb- and QD-antibody conjugates with constant concentrations leads to an increasing FRET sensitization of the QDs (PL measured in the QD650 detection channel: 660 ± 13 nm, left) and an increasing FRET quenching of the Tb (PL measured in the Tb detection channel: 494 ± 20 nm, right). Left: Black QD curve containing no PSA is composed of a short QD component (in the microsecond range) from direct QD excitation and a long Tb component (in the millisecond range) from spectral cross-talk of Tb in the QD detection channel. A new FRET decay time component (in the tens to hundreds of microseconds range) with increasing intensity (from red to blue) becomes clearly visible once Tb and QD are brought in close proximity due to the antibody−PSA binding. Right: Black Tb curve without PSA contains only long-lived Tb emission (no QD PL cross-talk in this channel), which is FRET-quenched (decreased PL decay time) due to antibody−PSA binding. PL decay curves for all other antibody combinations shown in Scheme 1 can be found in the Supporting Information.

(CV) because the ratiometric measurement intrinsically corrects for medium interferences. Within the assays, 50 μL of serum was mixed with 100 μL of AB conjugate solution (50 μL of Tb and QD conjugate each at a constant concentration). Apart from PSA-free serum, 18 serum samples with PSA concentrations ranging from 0.6 to 36 nM were measured. Each measurement takes 5 s per sample. Figure 3 shows the assay calibration curves achieved with these different concentrations. All assay curves show a strong increase of F_R with increasing PSA concentrations until *ca.* 10−20 nM PSA, which is the concentration range, where the ABs (QD and/or Tb conjugates) become saturated by PSA biomarkers and higher PSA concentrations do not provide additional FRET. It should be noted that the concentrations of Tb and QD are constant for all samples, which means that the increase of the time-gated FRET ratio is caused by FRET sensitization of QDs by Tb (the increase of F_R cannot be caused by nonspecific signals, *e.g.*, due to an increasing QD or Tb concentration). For most samples, the so-called "hook-effect" becomes apparent at even higher concentrations, where an excess of PSA leads to a stronger formation of individual "(Tb-AB)-PSA" and "(QD-AB)-PSA" complexes (compared to the "(Tb-AB)-PSA-(QD-AB)" FRET complexes), and thus a decreasing F_R is observed.[41] In order to distinguish the F_R values of the increasing slope (concentrations before the hook-effect) from the decreasing slope (concentrations after the hook-effect), the automated KRYPTOR plate reader system performs a kinetic measurement. This means that the system measures F_R directly after the addition of the serum sample to the AB conjugate solutions and then every few minutes in order to evaluate the increase of F_R over time. Using the calibration curve for the specific assay (in our case PSA), the system knows the highest value for the dynamic range (saturation of F_R in the curves in Figure 3) and can automatically dilute the sample in case the sample concentration is too high. Although we have not used the automated pipetting, this feature is a standard tool on the KRYPTOR compact clinical plate reader. Apart from avoiding problems with the hook-effect, the automated and calibrated dilution (using kinetic measurements) allows for a much larger dynamic range because also highly concentrated samples can be analyzed.

The QD-IgG assay curve differs from the others in that the curvature is rather of sigmoidal shape. This is consistent with our previous observation that an efficient separation of free IgG from the QD-IgG conjugates after labeling is difficult due to the similar sizes of QD and IgG. The shape of the red assay curve in Figure 3 is most probably caused by a small amount of free IgG antibodies, which are still present in the QD-IgG conjugate solution. These free ABs will participate in binding but not in energy transfer, and thus the initial increase of F_R is less steep compared to the QD conjugates with the smaller AB fragments, for which separation is much easier using spin column purification. The assumption of free ABs in the QD-IgG conjugate solution is further supported by the QD605 assay curve (Figure 3 right), for which a lower labeling ratio of *ca.* 0.5 AB/QD605 was used. In this configuration, there are free QDs (and no free ABs) in the QD605 conjugate solution, which is unproblematic for time-gated FRET detection (free acceptor fluorophores do not contribute to the FRET signal).[21] The increase of F_R with increasing PSA concentration shows a similar shape to the QD650 conjugates of fragmented ABs. However, it should be noted that the increase is less steep because the lower labeling ratio leads to less

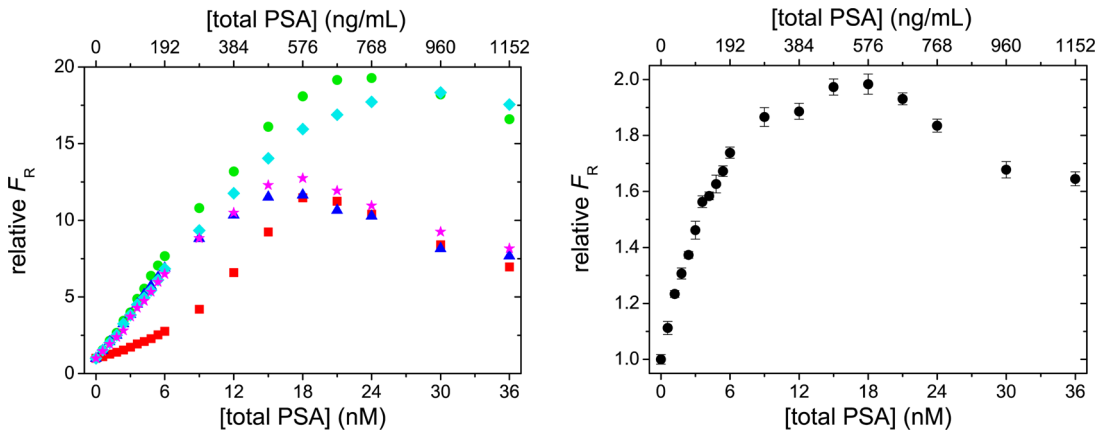

Figure 3. Tb-to-QD time-gated homogeneous FRET PSA immunoassays. Left (QD650): Relative time-gated (0.1−0.9 ms) PL intensity ratios (F_R normalized to unity at [total PSA] = 0) as a function of total PSA concentration. The selected antibody pairs were IgG + IgG (red squares), IgG + F(ab′)$_2$ (green dots), IgG + F(ab) (blue triangles), F(ab′)$_2$ + F(ab′)$_2$ (cyan rhombi), and F(ab) + F(ab) (magenta stars) for Tb and QD650, respectively. Increasing PSA concentrations led to a strong increase of F_R for all antibody combinations with a linear detection range spanning *ca.* 3 orders of magnitude for the F(ab′)$_2$ systems. For intercomparison, all curves were measured under the same experimental conditions. Right (QD605): Relative F_R values of the "(Tb-IgG)-PSA-(QD-IgG)" pair show a similar behavior to the QD650-based FRET systems and demonstrate the feasibility of a QD-based multiplexed homogeneous immunoassay. Limits of detection (LODs) for the assays can be found in Table 2.

TABLE 2. Limits of Detection (LODs), Dynamic Range, and Maximum Coefficients of Variation (CV_{max}) for the Different Homogeneous FRET Immunoassays[a]

Tb conjugate	QD conjugate	LOD (nM)	saturation (nM)	LOD (ng/mL)	LOD (fmol)	CV_{max} (%)
Tb-IgG	QD650-IgG	0.27	18	8.4	13.0	1.9
Tb-IgG	QD650-F(ab′)$_2$	0.06	21	1.8	2.8	1.8
Tb-IgG	QD650-F(ab)	0.05	15	1.6	2.5	0.7
Tb-F(ab′)$_2$	QD650-F(ab′)$_2$	0.08	21	2.6	4.1	2.6
Tb-F(ab)	QD650-F(ab)	0.05	15	1.6	2.5	0.6
Tb-IgG	QD605-IgG	0.25	15	7.9	12.0	1.3

[a] LODs of PSA are given for the 50 μL serum samples (LODs in the complete 150 μL measurement volume are 3 times lower). Saturation concentrations (the concentrations for which the PL intensity ratios in Figure 3 do not further increase) determine the dynamic range (which lies between the LOD and the saturation value). LODs were determined using the calibration curve concentration corresponding to the average F_R value plus 3 times its standard deviation of 30 serum samples containing no PSA (zero biomarker samples). The fmol LOD values were determined for a volume of 50 μL. The maximum coefficients of variation (CV_{max}) are given for the 30 serum samples containing no PSA. CVs for all samples containing PSA were below that maximum value. All values have an error of approximately 20%.

FRET signal per AB. We also note that carefully optimized ultracentrifugation or gel filtration chromatography might lead to better purification results of the QD-IgG conjugates. However, we wanted to demonstrate improved separation of small AB fragments using similar conditions for all QD-AB conjugates, in particular, by using convenient spin column purification, which can be performed using a standard laboratory benchtop centrifuge.

The limits of detection (LODs; cf. Table 2) of all homogeneous FRET assays are in the subnanomolar (few ng/mL) PSA range, and the dynamic range spans approximately 2 to 3 orders of magnitude. As expected from Table 1, the LODs are favorable for the AB-fragment-containing QD conjugates. The difference of ABs for the Tb conjugates is negligible, which we attribute to the relatively large distances in our sandwich immunoassay (Tb donors labeled to the Fc region of the IgG are too far away from the QD acceptor to participate in efficient FRET). Although the difference in LOD from QD650-IgG to QD650-F(ab′)$_2$ and QD650-F(ab) is quite significant (0.27 nM compared to 0.06 and 0.05 nM), there is only a minor difference between QD-F(ab′)$_2$ and QD-F(ab). As already mentioned above, there might be two main reasons for this. First, a high labeling ratio might lead to steric hindrance for Tb-AB binding *via* PSA. Second, F(ab) contains only one binding site (whereas IgG and F(ab′)$_2$ contain two), and the random orientation as well as the reduced affinity might lead to lower binding efficiencies per AB. In other words, the advantages of the small F(ab)s (compared to F(ab′)$_2$) are compensated by their disadvantages. Thus, both F(ab′)$_2$ and F(ab) are very well-suited for our Tb-to-QD FRET immunoassays.

Another remarkable aspect concerns the very low coefficients of variation for the QD-F(ab)-containing FRET systems. This important advantage is most probably caused by the higher labeling ratio of the small F(ab) fragments per QD, which leads to a lower background signal of directly excited QDs per "(Tb-AB)-PSA-(QD-AB)" binding (more FRET pairs per QD because multiple Tb can excite one QD in a serial manner due to

the large difference in excited-state lifetimes as explained above). Therefore, the fluorescence reader system can be used at a higher detector sensitivity without detector saturation. The best immunoassay system combining maximum sensitivity (minimum LOD), minimum antibody modification (no IgG reduction for the Tb conjugates), and maximum separation efficiency is therefore the "(Tb-IgG)+(QD-F(ab))" system.

CONCLUSIONS

In this study, we examine the application of Tb-to-QD FRET in a time-gated homogeneous immunoassay for PSA. We note that Chen *et al.* reported an initial demonstration where they used FRET from self-made Tb complexes to QD-doped microparticles for a homogeneous detection of α-fetoprotein.[31] However, in this preliminary study, the authors only presented a superficial photophysical analysis of the FRET processes and performed the assays in buffer. In contrast, we present (1) a full photophysical study of all pertinent FRET components and processes; (2) the use of two stable and biocompatible QDs with different colors; (3) a full characterization of assays using three types of antibodies (IgG, $F(ab')_2$, and F(ab)); and (4) high sensitivity in serum samples, which is the medium of relevance for diagnostic applications with minimal sample preparation.

We find that the PL decays of both Tb- and QD-antibody conjugates with and without PSA give clear evidence of PSA-binding-induced FRET from Tb to QD. The FRET ratio F_R can be used to sensitively and accurately determine biomarker concentrations at clinically relevant concentrations in small-volume serum samples. In the case of the PSA assay presented here, the LOD of 1.6 ng/mL (Table 2) is well below the commonly used serum PSA cutoff value of 4 ng/mL and even below the 2 ng/mL cutoff value proposed for higher-sensitivity PSA diagnosis.[42] Apart from PSA, the homogeneous Tb-to-QD FRET immunoassay is suitable for any other biomarker for which two specific IgG antibodies exist. Our flexible bioconjugation strategy offers facile assembly and purification of the Tb- and QD-AB conjugates, where the highest sensitivity assay (lowest LOD) resulted from F(ab)-based QD conjugates, due to higher Tb/QD pairs at closer donor−acceptor distances. To our knowledge, this is the first QD-based immunoassay to combine successfully all 11 attributes of an ideal homogeneous assay (as enumerated in the introduction) for real-life clinical diagnostics. Although our detection limits are very low and in a clinically relevant concentration range, it should be noted that commercial assays (*e.g.*, the standard KRYPTOR total PSA kit) still provide lower LODs. Nevertheless, these assays are fully optimized commercial immunoassay kits, and they use conventional fluorophores as FRET acceptors, which limit their multiplexing capability. Therefore, such assays do not exist as multiplexed kits. Our demonstration of replacing such standard fluorophores with QDs for homogeneous FRET immunoassays in combination with our recent work on highly increased sensitivity and multiplexing using up to five different biomarkers[18,19] strongly suggests that further development and optimization of Tb-to-QD FRET immunoassays will soon generate multiplexed diagnostic kits with even lower LODs for fast, flexible, and efficient early disease detection.

MATERIALS AND METHODS

Antibodies. The anti-PSA IgGs "PSR222" and "PSS233" were provided by Cezanne/Thermo Fisher Scientific. F(ab) and $F(ab')_2$ fragments of IgGs were generated using Pierce Mouse IgG1 F(ab) and $F(ab')_2$ preparation kit (Thermo Fisher Scientific). Fragmentation was verified using SDS-PAGE.

QD-Antibody Conjugates. eFluor650/605 nanocrystal conjugation kit−sulfhydryl reactive (provided by eBioscience in lyophilized form) was used for all QD conjugations. Details of the conjugation chemistry are described in ref 34. Antibody solutions (in concentration access compared to the QD solutions) were prepared in 1× PBS and conjugated to QDs according to the manufacturer's instructions. Unbound proteins were separated by washing 3−6 times in 100 kDa molecular weight cutoff (MWCO) spin columns (Millipore) with 100 mM sodium tetraborate buffer (pH 8.3) as the wash buffer. QD concentrations were determined by absorbance measurements using molar absorptivities of $1.1 \times 10^6\ M^{-1}\ cm^{-1}$ (at 641 nm) for QD650 and of $2.5 \times 10^5\ M^{-1}\ cm^{-1}$ (at 594 nm) for QD605 as provided by the manufacturer. Antibodies were quantified by absorbance measurements at 280 nm using molar absorptivities of 210 000, 140 000, and 70 000 $M^{-1}\ cm^{-1}$ for IgG, $F(ab')_2$, and F(ab), respectively. The labeling ratios were determined by linear combination of the respective absorbance values of QDs and antibodies within the QD-antibody conjugates.

Tb-Antibody Conjugates. Lumi4-Tb-NHS (provided by Lumiphore in lyophilized form) was dissolved to 8 mM in anhydrous DMF and mixed (in concentration excess to the antibody solutions) with the antibody samples in 100 mM carbonate buffer at pH 9.0. The mixtures were incubated while rotating at 25 rpm (Intelli-Mixer, ELMI) for 2 h at room temperature. For Tb-antibody conjugate purification, the samples were washed 4−6 times with 100 mM Tris-Cl pH 7.2 using 10 kDa MWCO spin columns (Millipore) for both $F(ab')_2$ and F(ab), and 50 kDa MWCO spin columns for IgG. Tb concentrations were determined by absorbance measurements at 340 nm using a molar absorptivity of 26 000 $M^{-1}\ cm^{-1}$ as provided by the manufacturer. Antibodies were quantified by absorbance measurements at 280 nm. The labeling ratios were determined by linear combination of the respective absorbance values of Tb and antibodies within the Tb-antibody conjugates.

Optical Characterization. Absorption spectra (Lambda 35 UV/vis System, PerkinElmer) and emission spectra (FluoTime 300, PicoQuant) were recorded in tris(hydroxymethyl)aminomethane (Tris-Cl, Sigma Aldrich) buffer with a pH of 7.4 and sodium tetraborate buffer with a pH of 8.5 (Sigma Aldrich) for Tb and QD samples, respectively. PL quantum yields and Förster distances were determined as described elsewhere.[40] PL decay curves were acquired directly from the FRET immunoassay samples (*vide infra*) on an EI fluorescence plate reader (Edinburgh Instruments) using 4000 detection bins of 2 μs integration time and nitrogen laser (VSL 337 ND, Spectra Physics) excitation (337.1 nm, 20 Hz). Optical transmission filter band-pass wavelengths were 494 ± 20 nm (Semrock) for the Tb detection channel, 660 ± 13 nm (Semrock) for the QD650 detection channel, and 607 ± 8 nm (Delta) for the QD605 detection channel.

Homogeneous FRET Immunoassays. The Tb- and QD-antibody conjugates were each dissolved in 50 μL Tris-Cl buffer containing 0.5% bovine serum albumin (BSA, Sigma-Aldrich). The concentrations (of the ABs; for the Tb and QD concentrations, see labeling ratios in the article) were approximately 6.9 nM for the Tb-IgG, 11.4 nM for the Tb-F(ab′)$_2$, 16.2 nM for the Tb-F(ab), 12.6 nM for the QD650-IgG, 11.7 nM for the QD650-F(ab′)$_2$, 23.1 nM for the QD650-F(ab), and 2.1 nM for the QD605-IgG. Then, 50 μL serum samples (added to the 100 μL solutions containing both the Tb and QD conjugates) were prepared from a stock solution of normal human serum containing 69.7 μg/mL PSA by dilution with purified newborn calf serum (both provided by Cezanne/Thermo Fisher Scientific) to yield the desired PSA concentrations. Serum without PSA was pure newborn calf serum. Time-gated (0.1−0.9 ms) PL intensity measurements were acquired on a KRYPTOR compact plus fluorescence plate reader (Cezanne/Thermo Fisher Scientific) using 500 detection bins of 2 μs integration time and nitrogen laser excitation (337.1 nm, 20 Hz, 100 pulses). Optical transmission filter band-pass wavelengths were 494 ± 20 nm (Semrock) for the Tb detection channel, 660 ± 13 nm (Semrock) for the QD650 detection channel, and 607 ± 10 nm (Delta) for the QD605 detection channel. All FRET assays were measured in black 96-well microtiter plates with an optimal working volume of 150 μL. Each sample containing PSA serum samples was prepared three times, and the samples without PSA were prepared 10 times. All samples were measured in triplicate. After sample preparation, the microtiter plates were incubated for 120 min at 37 °C before measurements on the KRYPTOR and EI fluorescence plate readers.

Conflict of Interest: The authors declare no competing financial interest.

Acknowledgment. The authors thank Lumiphore, Inc. for the gift of Lumi4-Tb-NHS reagent, and the European Commission (FP7 project NANOGNOSTICS), the European Innovative Medicines Initiative IMI (project OncoTrack), the Investissements d'Avenir Program France (project NanoCTC), and the Agence National de la Recherche France (project NanoFRET) for financial support.

Supporting Information Available: PL decay curves of the following FRET immunoassays: (1) the "(Tb-IgG)-PSA-(QD650-IgG)", (2) "(Tb-IgG)-PSA-(QD650-F(ab′)$_2$)", (3) "(Tb-IgG)-PSA-(QD650-F(ab))", (4) "(Tb-F(ab))-PSA-(QD650-F(ab))", and (5) "(Tb-IgG)-PSA-(QD605-IgG)". This material is available free of charge *via* the Internet at http://pubs.acs.org.

REFERENCES AND NOTES

1. Select Biosciences Market Report: *Mutiplexed Diagnostics 2010*, May 2010, Sudbury, UK.
2. Jain, K. K. Applications of Nanobiotechnology in Clinical Diagnostics. *Clin. Chem.* **2007**, *53*, 2002–2009.
3. Hötzer, B.; Medintz, I. L.; Hildebrandt, N. Fluorescence in Nanobiotechnology: Sophisticated Fluorophores for Novel Applications. *Small* **2012**, *8*, 2297–2326.
4. Algar, W. R.; Susumu, K.; Delehanty, J. B.; Medintz, I. L. Semiconductor Quantum Dots in Bioanalysis: Crossing the Valley of Death. *Anal. Chem.* **2011**, *83*, 8826–8837.
5. Gill, R.; Zayats, M.; Willner, I. Semiconductor Quantum Dots for Bioanalysis. *Angew. Chem., Int. Ed.* **2008**, *47*, 7602–7625.
6. Kuang, H.; Zhao, Y.; Ma, W.; Xu, L.; Wang, L.; Xu, C. Recent Developments in Analytical Applications of Quantum Dots. *TrAC, Trends Anal. Chem.* **2011**, *30*, 1620–1636.
7. Medintz, I. L.; Uyeda, H. T.; Goldman, E. R.; Mattoussi, H. Quantum Dot Bioconjugates for Imaging, Labelling and Sensing. *Nat. Mater.* **2005**, *4*, 435–446.
8. Rosenthal, S. J.; Chang, J. C.; Kovtun, O.; McBride, J. R.; Tomlinson, I. D. Biocompatible Quantum Dots for Biological Applications. *Chem. Biol.* **2011**, *18*, 10–24.
9. Alivisatos, A. P. Semiconductor Clusters, Nanocrystals, and Quantum Dots. *Science* **1996**, *271*, 933–937.
10. Alivisatos, P. The Use of Nanocrystals in Biological Detection. *Nat. Biotechnol.* **2004**, *22*, 47–52.
11. Chan, W. C. W.; Nie, S. M. Quantum Dot Bioconjugates for Ultrasensitive Nonisotopic Detection. *Science* **1998**, *281*, 2016–2018.
12. Han, M. Y.; Gao, X. H.; Su, J. Z.; Nie, S. Quantum-Dot-Tagged Microbeads for Multiplexed Optical Coding of Biomolecules. *Nat. Biotechnol.* **2001**, *19*, 631–635.
13. Resch-Genger, U.; Grabolle, M.; Cavaliere-Jaricot, S.; Nitschke, R.; Nann, T. Quantum Dots *versus* Organic Dyes as Fluorescent Labels. *Nat. Methods* **2008**, *5*, 763–775.
14. Jin, Z.; Hildebrandt, N. Semiconductor Quantum Dots for *In Vitro* Diagnostics and Cellular Imaging. *Trends Biotechnol.* **2012**, *30*, 394–403.
15. Hildebrandt, N. Biofunctional Quantum Dots: Controlled Conjugation for Multiplexed Biosensors. *ACS Nano* **2011**, *5*, 5286–5290.
16. Algar, W. R.; Malanoski, A. P.; Susumu, K.; Stewart, M. H.; Hildebrandt, N.; Medintz, I. L. Multiplexed Tracking of Protease Activity Using a Single Color of Quantum Dot Vector and a Time-Gated Förster Resonance Energy Transfer Relay. *Anal. Chem.* **2012**, *84*, 10136–10146.
17. Algar, W. R.; Wegner, D.; Huston, A. L.; Blanco-Canosa, J. B.; Stewart, M. H.; Armstrong, A.; Dawson, P. E.; Hildebrandt, N.; Medintz, I. L. Quantum Dots as Simultaneous Acceptors and Donors in Time-Gated Förster Resonance Energy Transfer Relays: Characterization and Biosensing. *J. Am. Chem. Soc.* **2012**, *134*, 1876–1891.
18. Geißler, D.; Charbonnière, L. J.; Ziessel, R. F.; Butlin, N. G.; Löhmannsröben, H.-G.; Hildebrandt, N. Quantum Dot Biosensors for Ultrasensitive Multiplexed Diagnostics. *Angew. Chem., Int. Ed.* **2010**, *49*, 1396–1401.
19. Geißler, D.; Stufler, S.; Löhmannsröben, H.-G.; Hildebrandt, N. Six-Color Time-Resolved Förster Resonance Energy Transfer for Ultrasensitive Multiplexed Biosensing. *J. Am. Chem. Soc.* **2013**, *135*, 1102–1109.
20. Charbonnière, L. J.; Hildebrandt, N. Lanthanide Complexes and Quantum Dots: A Bright Wedding for Resonance Energy Transfer. *Eur. J. Inorg. Chem.* **2008**, 3241–3251.
21. Geißler, D.; Hildebrandt, N. Lanthanide Complexes in FRET Applications. *Curr. Inorg. Chem.* **2011**, *1*, 17–35.
22. Esteve-Turrillas, F. A.; Abad-Fuentes, A. Applications of Quantum Dots as Probes in Immunosensing of Small-Sized Analytes. *Biosens. Bioelectron.* **2013**, *41*, 12–29.
23. Ge, S.; Ge, L.; Yan, M.; Song, X.; Yu, J.; Liu, S. A Disposable Immunosensor Device for Point-of-Care Test of Tumor Marker Based on Copper-Mediated Amplification. *Biosens. Bioelectron.* **2013**, *43*, 425–31.
24. Härmä, H.; Soukka, T.; Shavel, A.; Gaponik, N.; Weller, H. Luminescent Energy Transfer between Cadmium Telluride Nanoparticle and Lanthanide(III) Chelate in Competitive Bioaffinity Assays of Biotin and Estradiol. *Anal. Chim. Acta* **2007**, *604*, 177–183.
25. Kattke, M. D.; Gao, E. J.; Sapsford, K. E.; Stephenson, L. D.; Kumar, A. FRET-Based Quantum Dot Immunoassay for Rapid and Sensitive Detection of *Aspergillus amstelodami*. *Sensors (Basel, Switzerland)* **2011**, *11*, 6396–6410.
26. Long, F.; Gu, C.; Gu, A. Z.; Shi, H. Quantum Dot/Carrier-Protein/Haptens Conjugate as a Detection Nanobioprobe for FRET-Based Immunoassay of Small Analytes with All-Fiber Microfluidic Biosensing Platform. *Anal. Chem.* **2012**, *84*, 3646–3653.
27. Qian, J.; Wang, C.; Pan, X.; Liu, S. A High-Throughput Homogeneous Immunoassay Based on Förster Resonance Energy Transfer between Quantum Dots and Gold Nanoparticles. *Anal. Chim. Acta* **2013**, *763*, 43–49.
28. Wei, O. D.; Lee, M.; Yu, X.; Lee, E. K.; Seong, G. H.; Choo, J.; Cho, Y. W. Development of an Open Sandwich Fluoroimmunoassay Based on Fluorescence Resonance Energy Transfer. *Anal. Biochem.* **2006**, *358*, 31–37.
29. Zeng, Q. H.; Zhang, Y. L.; Liu, X. M.; Tu, L. P.; Kong, X. G.; Zhang, H. Multiple Homogeneous Immunoassays Based on a Quantum Dots−Gold Nanorods FRET Nanoplatform. *Chem. Commun.* **2012**, *48*, 1781–1783.
30. Zhang, C. L.; Gao, D.; Zhou, G. H.; Chen, L.; Zhang, X. A.; Cui, Z. Q.; He, Z. K. Label-Free Homogeneous Immunosensor Based on FRET for the Detection of Virus Antibody in Serum. *Chem.—Asian. J.* **2012**, *7*, 1764–1767.
31. Chen, M. J.; Wu, Y. S.; Lin, G. F.; Hou, J. Y.; Li, M.; Liu, T. C. Quantum-Dot-Based Homogeneous Time-Resolved

Fluoroimmunoassay of α-Fetoprotein. *Anal. Chim. Acta* **2012**, *741*, 100–105.
32. Xu, J.; Corneillie, T. M.; Moore, E. G.; Law, G.-L.; Butlin, N. G.; Raymond, K. N. Octadentate Cages of Tb(III) 2-Hydroxyisophthalamides: A New Standard for Luminescent Lanthanide Labels. *J. Am. Chem. Soc.* **2011**, *133*, 19900–19910.
33. Hermanson, G. T. *Bioconjugate Techniques*, 2nd ed.; Academic Press: San Diego, CA, 2008.
34. Jennings, T. L.; Becker-Catania, S. G.; Triulzi, R. C.; Tao, G.; Scott, B.; Sapsford, K. E.; Spindel, S.; Oh, E.; Jain, V.; Delehanty, J. B.; *et al.* Reactive Semiconductor Nanocrystals for Chemoselective Biolabeling and Multiplexed Analysis. *ACS Nano* **2011**, *5*, 5579–5593.
35. Algar, W. R.; Kim, H.; Medintz, I. L.; Hildebrandt, N. Emerging Non-traditional Förster Resonance Energy Transfer Configurations with Semiconductor Quantum Dots: Investigations and Applications. *Coord. Chem. Rev.* **2013**http://dx.doi.org/10.1016/j.ccr.2013.07.015.
36. Charbonniere, L. J.; Hildebrandt, N.; Ziessel, R. F.; Löhmannsröben, H.-G. Lanthanides to Quantum Dots Resonance Energy Transfer in Time-Resolved Fluoro-immunoassays and Luminescence Microscopy. *J. Am. Chem. Soc.* **2006**, *128*, 12800–12809.
37. Hildebrandt, N.; Charbonniere, L. J.; Beck, M.; Ziessel, R. F.; Löhmannsröben, H.-G. Quantum Dots as Efficient Energy Acceptors in a Time-Resolved Fluoroimmunoassay. *Angew. Chem., Int. Ed.* **2005**, *44*, 7612–7615.
38. Hildebrandt, N.; Charbonniere, L. J.; Löhmannsröben, H.-G. Time-Resolved Analysis of a Highly Sensitive Förster Resonance Energy Transfer Immunoassay Using Terbium Complexes as Donors and Quantum Dots as Acceptors. *J. Biomed. Biotechnol.* **2007**No. 79169.
39. Morgner, F.; Geißler, D.; Stufler, S.; Butlin, N. G.; Löhmannsröben, H.-G.; Hildebrandt, N. A Quantum-Dot-Based Molecular Ruler for Multiplexed Optical Analysis. *Angew. Chem., Int. Ed.* **2010**, *49*, 7570–7574.
40. Wegner, K. D.; Lanh, P. T.; Jennings, T.; Oh, E.; Vaibhav, J.; Fairclough, S. M.; Smith, J. M.; Giovanelli, E.; Lequeux, N.; Pons, T.; *et al.* Influence of Luminescence Quantum Yield, Surface Coating, and Functionalization of Quantum Dots on the Sensitivity of Time-Resolved FRET Bioassays. *ACS Appl. Mater. Interfaces* **2013**, *5*, 2881–2892.
41. Wild, D. *The Immunoassay Handbook*, 4th ed.; Elsevier: Amsterdam, 2013.
42. Greene, K. L.; Albertsen, P. C.; Babaian, R. J.; Carter, H. B.; Gann, P. H.; Han, M.; Kuban, D. A.; Sartor, A. O.; Stanford, J. L.; Zietman, A.; *et al.* Prostate Specific Antigen Best Practice Statement: 2009 Update. *J. Urol.* **2013**, *189*, S2–S11.